IN-FLIGHT DETECTION OF FLOW SEPARATION, STAGNATION, AND TRANSITION

S.M. Mangalam & S. Kuppa
Analytical Services & Materials, Inc.
Hampton, VA 23666

Abstract

Flight tests were conducted to demonstrate the feasibility of simultaneous determination of:

(a) boundary-layer instability and transition characteristics;

(b) flow separation region; and

(c) the location of the leading-edge stagnation point.

Surface mounted, multi-element, micro-thin, hot-film sensors were used in conjunction with a bank of constant-temperature anemometers and a PC-based 8-channel simultaneous data acquisition system. Conventional techniques were used to determine the boundary-layer instability and transition characteristics while the flow separation and the stagnation points were determined through the presence of phase reversal signatures.

Introduction

The aerodynamic performance of a flight vehicle critically depends on the state of the boundary layer on its lifting and non-lifting surfaces. A dramatic increase in aircraft range and endurance can be realized by maintaining an extensive region of laminar boundary layer which results in a significant reduction in drag and an increase in its lift-to-drag ratio [1-3] (see reference 4.for a recent survey on this subject). The presence of flow separation can lead to significant increase in drag and a consequent deterioration in aircraft performance. These boundary-layer characteristics become particularly significant for high-speed transport aircraft. Accurate demarcation of the state of the boundary layer in flight is essential for improved aircraft design and flight research. The demarcation of the laminar, transitional, and turbulent zones and their detailed characteristics would also be valuable for the verification of Computational Fluid Dynamics codes and models.

The determination of boundary-layer transition and flow separation in both wind tunnel and flight experiments has occupied the attention of researchers for decades. Sophisticated flow visualization techniques such as liquid crystals [5,6] and infrared imaging [7] have been extensively used to obtain qualitative information on transition. The analysis of the response history from hot-wire or hot-film sensors is an established method of determining the laminar (low amplitude, low rms), transitional (high intermittence, peak rms), and turbulent (high intermittence, high rms) regions of the boundary layer. For a recent survey of the research on transition, see reference 8. Furthermore, while the turbulent boundary layer is characterized by a broad-band spectrum, most of the energy in a laminar boundary layer is contained in the low frequency end of the energy spectrum. Thus, boundary-layer transition is conventionally determined on the basis of one or more of the following: (a) the amplitude of raw signals from the sensors; (b) the rms voltage levels of the sensor signals; (c) the spectral content of the signals; and (d) intermittency factor [9]. Heated film gages operated with constant-temperature anemometers have been widely used to detect the onset and the extent of transition in subsonic and supersonic flows [10-15]. Flush-mounted hot-film gages have also been extensively used in flight test research [15-22]. Flush-mounted hot-film gages which gave a measure of heat transfer and shear stress fluctuations at the surface became the sensor of choice for transition detection and for the determination of heat transfer and skin friction.

A breakthrough in flow diagnostics was accomplished by Mangalam and Stack in 1986 with the discovery of the phase reversal signature at the laminar separation point on an airfoil [15]. When the phase relations between signals from surface hot-film sensors were compared, it was found that there was a phase shift of 180° between the signals from sensors located across the separation point. The first author followed this discovery with a series of wind tunnel tests to determine the flow separation and reattachment points on airfoils, and the technique was later extended to the determination of shock location [14, 23-26]. The first author also developed a physical model for the occurrence of the phase reversal signature and successfully verified it with tests conducted to determine the stagnation point on a circular cylinder[13].

In parallel, further advances were made by Mangalam and his team to integrate the instrumentation system with PC-based data acquisition hardware and analysis software [27]. This system consists of multi-element thin-film sensors, a bank of constant-temperature anemometers, the data acquisition system, and a data analysis software for flow diagnostics. A number of studies (Table I) were conducted with this system to capture boundary-layer characteristics. The PC-based data acquisition and instrumentation system (DAISy) was modified for flight tests on a sailplane to simultaneously determine the boundary-layer characteristics and the stagnation point location[22].

Experimental Tools and the Flight Vehicle

The Aircraft

The flight tests were conducted on an AS-K21 sailplane [22]. This two place, fiber glass sailplane has a clean wing with a proprietary Wortmann airfoil designed to provide laminar flow up to about the mid-chord region at design conditions. Rapid transition to

turbulence occurs downstream to ensure a good pressure recovery. Laminar separation occurs at off-design conditions. This vehicle was thus well suited to establish the boundary-layer flow diagnostics techniques.

The in-flight flow diagnostics installation required no structural changes to the aircraft, no modifications or changes to the aircraft pitot-static system or the aircraft control surfaces/linkages. Initial flights of the aircraft in its instrumented test configuration showed no unusual control or stability problems. An experimental Airworthiness Certificate was issued for the duration of the flight testing by the Federal Aviation Administration Office.

Flow Visualization

Prior to the installation of sensors, flow visualization was done with tufts placed on the wing surface to determine the best location for the multielement sensor on the wing. The tuft pattern was recorded by a video camera mounted on an existing vertical tail mount. Audio leads from the camera were routed along the fuselage into the cockpit to provide the pilot with a microphone capability. These flight tests indicated the presence of flow separation in the mid-chord region for low speed flight.

Data Acquisition, and Instrumentation System (DAISy)

The flight test data was acquired with DAISy which consisted of a portable computer with a hard disk, mouse, network card, and a custom designed data acquisition card [22]. The computer was powered by a DC/AC inverter operating off a dedicated set of batteries. The system also contained the data acquisition software and network software. The computer was capable of recording approximately 100 sets of data per flight. Each flight data set consisted of time-series signals from 64 sensors sampled in groups of 8. The hard disk was used to store the data during the flight test. The network card was used so that the data collected could be downloaded upon landing into a ground-based DAISy. A schematic of the flight test instrumentation is shown in Figure 1.

The Sensors

Two multi-element hot film sensors were mounted on the wing, one on the leading edge for stagnation point studies and the second in the mid-chord region for separation and transition measurements. The multi-element sensor (S_{ts}) to determine the transition and flow separation characteristics extended from 42.8% chord to 53.6% chord on the upper surface of the port wing, 1.22 m. outboard of the fuselage. This sensor was also used to obtain the boundary-layer instability characteristics and to study the influence of roughness on transition.

The second multi-element sensor (S_{sp}) was placed closer in-board on the starboard wing and was wrapped around the leading edge to determine the location of the stagnation point.

The configuration of the 60-element sensors used in the flight tests is shown in Figure 2. The multi-element sensor consists of an array of Nickel films, that have been electron-beam deposited onto a 50 μm polyimide substrate. Each Nickel film element is 0.9 mm long, 0.15 mm wide and .15 μm high. Copper-coated Nickel leads were used to provide wire attachment strips that were led into the cockpit. The element sensor spacing is about 2.5 mm which provides a measurement resolution of 0.17c% for a 1.42 m chord wing. This resolution is more than an order of magnitude better than that obtained with existing flight test techniques such as pressure measurements or flow visualization. The substrate was bonded onto the wing surface with artist spray adhesive so that the sensors were aligned in the streamwise direction. The sensors were then connected to a bank of constant-temperature anemometer bridges.

The Constant Temperature Anemometer System

The anemometers were setup to operate the sensors at an overheat of approximately 1.2. Since all the tests were conducted at low altitudes and low speeds, all anemometer adjustments were made on the ground and there was no need for further in-flight adjustments. The data record for each channel consisted of 2048 data points sampled at rates of 500 Hz, 5,000 Hz, and 10,000 Hz. These rates were selected by the pilot by means of three computer mouse buttons. An average of 30 data runs were made in each flight before landing. The behavior of the tufts near the sensor location when data was acquired was recorded by the video camera.

The DAISy instrumentation package and the power supply were installed in the rear cockpit using a specially built wooden pallet and secured with the existing five-point seat-belt system. The computer mouse was mounted on the instrument panel. In some tests a video camera mounted in the cockpit was used to directly record the flight conditions from the instrument panel.

The instrumentation package consisted of 16 individual constant-temperature anemometers, a 16 to 8 crossbar switch (multiplexer), signal conditioners, and a rechargeable gel-cell battery pack. This is shown in Figure 3. All of these were built into a special rack with suitable backplane cards designed and built for compactness and ease of installation in the sailplane. The front panel provided access to the adjustment controls for the bridge resistance, offset voltage, and cable compensation. The computer controlled crossbar switch allowed the selection of 8 simultaneous outputs from the 16 anemometer channels available. These were then routed to the signal conditioner through a low pass filter to prevent aliasing during sampling. This arrangement made it possible to acquire simultaneous signals from any 8 sensors. The multiplexer allowed 8 data groups to be acquired, thus providing a total of 64 signals in one acquisition cycle.

The Flight Test Results & Discussions

Eleven research flights were made. The purpose of each flight is listed in Table II. Each flight averaged about 20 minutes. The flight measurements were made at altitudes between 750 m and 2,000 m above mean sea-level.. Most were slow speed flights terminating in nonaccelerated stalls.

The instrumentation system was turned on during the take-off and the computer completed its boot-up process. The sailplane was towed to an altitude of 1,000 m above ground level. The video monitor showed the state of the wing tufts and so allowed the pilot to choose the right moment to acquire data. The audio connection to the camera was used by the pilot to note the flight conditions on the video tape.

The first type of flight maneuver was a steady, straight and level run at a trimmed airspeed. Runs were made at airspeeds from 40 to 80 knots in increments of 10 knots. The second set of flight maneuvers used are steady turns for the same range of airspeeds. For each data acquisition test condition, turns were made to both the left and to the right. The third type of maneuver used was the slow-entry stall. Data were acquired at each of the three sample rates for the stall maneuvers. Combinations of these flight maneuvers were also used in some flights. A brief description of the flight-test measurements, their analyses, and flow diagnostics are given in the following sections.

Boundary-layer Instability and Transition

In the operation of a typical constant-temperature anemometer (CTA), a high-gain electronic feedback network tries to maintain the flush-mounted sensor at a constant temperature [28] while the convective heat transfer in the boundary layer tends to cool it. If the boundary layer is laminar, the surface shear stress and the convective heat transfer levels are low and hence the voltage fluctuations to maintain a constant temperature are also low. Thus, the signals from a sensor in the laminar boundary layer will have a low amplitude, slightly above the electronic noise level. As the boundary layer becomes unstable, periodic turbulent bursts begin to appear with associated increase in the signal amplitude. The amplitude reaches a maximum at peak transition. It is followed by a slight decrease in the amplitude level in the turbulent region. A typical sequence of events from laminar-to-turbulent transition is shown in Figure 4. These time traces of signals from sensors are obtained simultaneously with the use of multi-element sensors and thus provides a convenient method to simultaneously demarcate the laminar, transitional, and turbulent regions in the flow.

Figures 5 & 6 present plots of the instances where most amplified disturbance frequencies leading to transition were observed. The frequency content of the signals was analyzed to characterize the boundary layer instability. A visual inspection of the data in Figure 5 indicates significant activity in the raw signal from sensor 6. The signal appears to have large amplitudes at certain frequencies. The power spectral density plots for the signals from sensors 4 and 6 (Figures 5(b) & (c)) show that the most amplified Tollmien-Schlichting (TS) frequency is approximately 650 Hz. in both cases. The airfoil co-ordinates were not available for the proprietary Wortmann airfoil and hence a theoretical analysis could not be made for comparison. The most amplified TS-disturbance frequency obtained at another flight condition is identified to be at about 1050 Hz from Figure 6. The data in Figure 5 was obtained at a speed of about 40 knots, while for Figure 6 it was about 50 knots.

The location of the beginning and end of transition from the raw signal data involved the following : (a) observation of gradual increase in the amplitudes across the frequency range, (b) the variation of intermittency factor, and (c) the variation of rms voltage of the sensor signals. Technique (a) is a visual inspection of the signals and tends to be subjective in fixing the locations.

Figure 7 shows signals from sensors 2-16 (flight 003.012). The signal amplitude begins to increase from sensor 8, marking the beginning of transition. Peak values are observed in the signals from sensor 14, indicating the end of transition. These trends are confirmed by the variation in their rms levels shown in Figure 8 which indicates that the beginning of transition was just downstream of sensor 6, positioned at 0.45c. The peak transition occurs at sensor 15, positioned at 0.482c.

The intermittency factors are shown in Figure 9. These factors confirm that the beginning of transition is at sensor 6, but the end of transition, as marked by an intermittency factor of one, occurs at sensor 14, positioned at 0.478c. Location of the end of transition, based on the intermittency factor, is the more accurate determination [9]. Thus, for this case (flight #3), the laminar boundary layer extends up to 0.45c, where transition begins. The transitional zone is located between 0.45c and 0.478c.

Laminar Flow Separation and Turbulent Reattachment

At the point of separation (or reattachment) , the dividing streamline emanates from (or attaches to) the body. Aside from reflecting the local laminar or turbulent nature of the flow, the shear stress signals contain information regarding the unsteady features of the external flow. These unsteady features can be due to various reasons including wake oscillations, body geometry and attitude changes, flow instability, etc. Fluctuations in the oncoming mean flow cause the dividing streamline to move back and forth about a mean location over contiguous sensor elements at regular time intervals. At the separation point itself, the shear stress is a minimum, i.e., the convective heat transfer is a minimum. As we move farther away from the separation point, the shear stress (convective heat transfer) is expected to increase monotonically. The closely spaced sensor elements measure the surface shear stress fluctuations. The movement of the point of local minimum shear stress over a surface, shows up as a fluctuation in the local shear stress. This movement is generally restricted to a very small region. When hot-film sensors are used in such a way that they cover the

region of the movement and are aligned with the line of the movement, the signals from the hot-films will reflect the movement. When the point of minimum shear stress is at one extreme the signal is a minimum from the hot-film at that point, while the signal from the hot-film at the other extreme has a local maximum at that instance. This situation is reversed when the point of minimum shear stress moves to the other extreme. Thus, the signals from the hot-films just beyond the extremities of the region will show a phase difference of 180°. Also, the signals from the hot-films within the region of the movement will show frequencies which are double that of the frequencies seen in the signals beyond the region.

When spectral analysis is used to examine the time traces, the following picture emerges :

- The presence of phase reversal signature between signals from sensors across the mean separation point.
- The presence of the first harmonic in the signal obtained from the sensor located at the separation point.
- The presence of a negative maximum in cross-correlation of signals from the sensors across the separation point.
- A reduction in the mean signal amplitude at the separation location.
- The presence of a dominant frequency in the signals from any or all of the sensors in the separation region.

True phase relations can be obtained only when signals are obtained through simultaneous measurements. The use of multielement sensors and the multi-channel, simultaneous data acquisition system enables us to ensure simultaneous measurements.

The important assumptions made in developing the above model are: (i) the boundary-layer is inherently unsteady which results in a spatial oscillation of the separation point, and (ii) the shear stress fluctuations are a minimum at the instantaneous separation point and increase monotonically, in the neighborhood, with distance from the separation point. Since the separation point is essentially a stagnation point, similar behavior should also be expected at the leading-edge stagnation point. This physical explanation for the phase reversal signature was verified in a wind-tunnel experiment [13]. Laminar flow separation point was determined in flight using the above described flow diagnostics technique based on the presence of phase reversal signature.

Figure 5(a) shows raw data from the first research flight, Run No. 12 (see Table II) where the measurement resolution was 0.67%c. In this representation of the data the phase reversal between signals is not apparent. These signals were processed using Fast Fourier Transform to perform spectral analysis on the signals. Phase angle, the quantity of interest from the spectral analysis, between hot-film signals 1-2, 2-3, 1-4, 4-5 and 5-6 are presented in Figure 10. A phase reversal can be observed between signals from sensors 2-3 and 1-4. Figure 10 also shows that signals from sensors 1-2 are in phase, as are 4-5 and 5-6. From this analysis it is clear that laminar boundary-layer is attached up to sensor 2 and separates between sensors 2 and 3. This corresponds to a position of .4485c on the wing S_{ts} sensor.

The Stagnation Point Location

The stagnation point location was obtained from the multi-element sensor wrapped around the leading edge. All signals from these sensors have low amplitudes as seen in Figure 11 showing the presence of a laminar boundary layer.

In order to extract the information on the location of the leading-edge stagnation point that must be present in these signals, the phase relations between adjacent pairs of sensor signals were examined for a phase reversal signature (PRS). Figure 11 shows time traces of signals from sensors 9-16 for Run 10, Flight 8. These signals show the unsteadiness of the flow in a relatively small amplitude. This is due to the inability of the anemometers employed in this study to give sufficient sensitivity and frequency response at the same time. However, a clear phase reversal is observed between the signals 13 and 14 which is evident from a closer look depicted in Fig. 11(b). The cross-spectral analysis plots, shown in Figure 12, for these signals confirm the presence of a phase reversal. Thus, for this flight condition, the leading-edge stagnation point lies between the sensors 13 and 14. The physical location of sensor 11 was the geometric center of the leading-edge curve of the wing. For comparison, the phase relations between other pairs of signals from sensors located on either side of the stagnation point are shown in Figs. 13 and 14 which clearly indicate that there is zero phase difference between them.

The stagnation point can be, in principle, related to the angle-of-attack of the wing. Changes in the aircraft attitude produce changes in the stagnation point location. The angle-of-attack was not measured but a significant change in stagnation point location was observed in these flight tests when the aircraft attitude was changed. Thus, the stagnation point moved from sensor No. 5 to sensor No. 15 for the range of angles-of-attack flown.Thus, the diagnostic technique described here can be used to find the stagnation point travel during maneuvers.

Roughness effects

The capability to locate forced transition was demonstrated with a sand particle used as a small three-dimensional roughness. The sand particle was glued to the multi-element sensor substrate. It was placed 1.3 mm outboard of the sensor array in the spanwise direction, it lay between sensor 3 and 4 in the chordwise direction. Raw signals from these sensors shown in Figure 15 clearly indicate laminar boundary-layer characteristics up to sensor 3 (small amplitude - mV range) and turbulent flow characteristics beyond (larger amplitude - 0 V -0.35 V range). The rms levels and intermittency factors are shown in Figure 16, confirming this observation. However, Figure 17 (a) shows the phase relations of the sensor signals indicating the presence of laminar separation between sensors 3 and 4. The use of the PRS technique shows that the turbulence has actually occurred in a separated shear layer. Figures 17 (b) & 17 (c) show the phase angle plots for signals from sensors 5 & 11 and 7 & 11 (sensor 9 was inoperative during this flight), indicating another phase reversal between sensors 7 & 11. This verifies

that turbulent attachment occurred in this region. The entire transformation, from an attached laminar boundary layer to laminar separation, transition, and turbulent reattachment took place within a chordwise distance of only 2 cm It is almost impossible to detect such minute details with other measurement techniques. Thus, the flow diagnostics technique based on phase reversal signatures is a powerful tool to detect the details of the state of the boundary layer, including the presence of flow separation and reattachment.

Conclusions

The flight tests clearly demonstrated the feasibility of simultaneous detection of boundary-layer separation and reattachment points as well as the stagnation points. The ability to demarcate the boundary layer transitional zone as well as the capability to detect the effects of artificially induced surface roughness on the boundary layer was demonstrated by the flow diagnostic tool. This was achieved by using the PRS technique along with the portable flow diagnostic DAISy. Flow separation and reattachment regions were located by using the PRS technique whereas transition was determined using conventional techniques.

The flight test study hence demonstrated that the following flow characteristics can be simultaneously determined in flight:

1) The location of the leading-edge stagnation point.
2) The location of boundary layer separation and reattachment points.
3) The frequencies of the most amplified Tollmien-Schlichting disturbances in unstable laminar boundary layers.
4) The influence of three-dimensional roughness on transition and separation.

Acknowledgments

This work was conducted under the NASA SBIR Program (Contract NAS2 - 13252) with Ms. Bianca Anderson of Ames-Dryden Flight Research Facility as the Technical Monitor.

References

1) Pfenninger, W.; Design Considerations of Large Global Range High Subsonic Speed LFC transport airplanes, AGARD/VKI Special Course on Concepts for Drag Reduction, Rhode-St. Genese, Belgium (1977), AGARD 654.

2) Anderson, B. T. and Meyer, R. R. ; Effects of Wing Sweep on In-Flight Boundary-Layer Transition for a Laminar Flow Wing at Mach Numbers From 0.60 to 0.79, NASA TM-101701, 1990.

3) Hefner, J.N. and Bushnell, D.M. ; An Overview of Concepts for Aircraft Drag Reduction, AGARD Rep. 654, June 1977, pp 1-1 to 1-30.

4) Bushnell, D. ; Supersonic Aircraft Drag Reduction, AIAA 90-1596, June 1990.

5) Holmes, B. J.; Croom, C. C.; Gall, P. D.; Manuel, G. S.; and Carraway, D. L.: Advanced Transition Measurement Methods for Flight Applications. AIAA Paper 89-9786, 1986.

6) Gall, P. D.; and Holmes, B. J.: Liquid Crystal for High-Altitude In-Flight Boundary Layer Flow Visualization, AIAA-83-2522.

7) Brandon, J.M., Manuel, G.S., Wright, R.E. and Holmes, B.J.: In-Flight Flow Visualization Using Infrared Imaging, AIAA Paper No. 88-2111, May 1988.

8) Arnal, D.: Boundary Layer Transition : Prediction, Application to Drag Reduction, AGARD FDP/VKI Special Course on "Skin Friction Drag Reduction", VKI, Brussels, Belgium, March 1992.

9) Dhawan, S. and Narasimha, R.: Some Properties of Boundary Layer Flow During Transition from Laminar to Turbulent Motion, Journal of Fluid Mechanics, Vol. 3, Pt. 4, 1958, pp. 418-436.

10) Owen, F. K.; and Bellhouse, B. J.: Skin Friction Measurements at Supersonic Speeds. AIAA Journal Vol. 8, 1970.

11) Bellhouse, B. J.; and Schultz, D. L.: Determination of Mean and Dynamic Skin Friction, Separation, and Transition in Low-Speed Flow with a Thin-Film Heated Element. Journal of Fluid Mechanics, vol. 24, pt. 2, 1966, pp. 379-400.

12) Mangalam, S. M.; Maddalon, D. V.; Saric, W. S.; and Agarwal, N. K.: Measurement of Crossflow Vortices, Attachment-line Flow, and Transition using Microthin Hot Films. AIAA 90-1636 (1990).

13) Mangalam, S. M. and Kubendran, L. R.: Experimental Observations on the Relationship between Stagnation Region Flow Oscillations and Eddy Shedding for Circular Cylinder, Proc. ICASE/NASA Instability and Transition Workshop (1989).

14) Mangalam, S. M.; Stack, J. P.; and Sewall, W. G.: Simultaneous Detection of Separation and Transition in Surface Shear Layers. Fluid Dynamics of Three-Dimensional Turbulent Shear Flows and Transition, AGARD-CP-438, 1988.

15) Manuel, G. S.; Carraway, D. L.; and Croom, C.C.: The Laminar Separation Sensor: An Advanced Transition Measurement Method for Use in Wind Tunnels and Flight. SAE TP 871018, 1987.

16) Chiles, H. R.; and Johnson, J. B.: Development of a Temperature-Compensated Hot-Film Anemometer System for Transition Detection on High-Performance Aircraft. NASA TM-86732, 1985.

17) Chiles, H. R.: The Design and Use of a Temperature-Compensated Hot-Film Anemometer System for Boundary-Layer Transition Detection on Supersonic Aircraft. NASA TM-100421, 1988.

18) Croom, C. C.; Manuel, G. S.; and Stack, J. P.: In-Flight Detection of Tollmien-Schlichting Instabilities in Laminar Flow. SAE Technical Paper Series 871016.

19) Hall, R.M., Obara, C.J., Carraway, D.L., Johnson, C.B., Wright, R.E., Covell., P.F., Azzazy, M.: Comparisons of Boundary-Layer Transition Measurement Techniques in the Langley Unitary Plan Wind Tunnel, AIAA Paper No. 89-2205, 1989.

20) Holmes, B. J.: Progress in Natural Laminar Flow Research, AIAA/NASA General Aviation Technology

Conference, Hampton, Virginia, July 1984.

21) Obara, C. J.; and Holmes, B. J.: Flight-Measured Laminar Boundary-Layer Transition Phenomena Including Stability Theory Analysis. NASA TP 2417, 1985.

22) Mangalam, S.M.; Wusk, M.S.; Kuppa, S.: In-Flight Detection of Stagnation, Transition and Separation Using Micro-thin Surface Hot-films, Society of Flight Test Engineers (SFTE) 22nd Annual Symposium, August 1991.

23) Sewall, W. G.; Stack, J. P.; McGhee, R. J.; and Mangalam, S.M.: A New Multipoint Thin-Film Diagnostic Technique for Fluid Dynamic Studies. SAE Technical Paper Series 881453.

24) Stack, J. P.; Mangalam, S. M; and Berry, S. A.; A Unique Technique to study Laminar-Separation Bubble Characteristics on an Airfoil. AIAA Paper 87-1271, 1987.

25) Stack, J. P.; Mangalam, S. M.; and Kalburgi, V.: Phase Reversal Phenomenon at Flow Separation and Reattachment. AIAA Paper 88-0408, 1988.

26) Stack, J.P. and Mangalam, S.M.: US Patents No.4,848,153(1989) and No.4,936,146(1990).

27) Mangalam, S. M.; Balister, R. L.; and Kubendran, L. R.: An Advanced PC-based Instrumentation System for Flow Diagnostics. Paper 90-123, Proc. of 36th International Instrumentation Symposium, Denver, CO (1990).

28) Perry, A. E.: Hotwire Anemometry. Oxford University Press, New York, 1982.

29) Lee, C.C.; Obara, C.J.; Vijgen, P.M.; and Wusk, M.S.: Flight Experiments Measuring Boundary-Layer Disturbances in Laminar Flow and Correlation with Stability Analysis, AIAA 91-1635, June 1991.

30) Lee, C.C.; Wusk, M.S.; and Obara, C.J. : Flight Experiments Studying the Growth of Disturbances in the Laminar Boundary Layer, SAE Technical Paper Series 901979, October 1990.

31) Agarwal, N.K.; Maddalon, D.V.; Mangalam, S.M.; and Collier, F.S. : Cross-flow Vortex Structure and Transition Measurements using Multi-Element Hot Films, AIAA 91-0166, January 1991.

Facility	Flow Feature Detected
NASA-Langley Shear Flow Tunnel (1989) - Cylinder	Stagnation - Shedding (Ref. 13)
Boeing (1989) - Swept Wing	Attachment Line Flow
RAE Farnborough (1989) - Swept Wing High-Lift Configuration	Attachment Line Flow
ASU (1990) - Swept Wing	Cross-flow, Attachment Line Flow (Ref. 12)
ASU (1991) - Swept Wing	Cross-flow, Attachment Line Flow (Ref. 29)
SBIR Flight Test (1990) - Sailplane	Separation, Instability, Transition, Stagnation (Ref. 22)
NASA-Langley Flight Test (1990)	Boundary-Layer Instability (Ref. 30)
NASA-Langley Flight Test (1991) - Lear Model 28/29	Boundary-Layer Disturbances (Ref. 31)

Table I. Wind Tunnel and Flight Tests conducted with DAISy.

Flt	Data Run # s	Speed Range	Description
1.	calct001.002-.036	40 - 60 knots	TSS, Alternate @4
2.	calct001.037-.056	40 - 60 knots	TSS, Alternate @4
3.	calct003.000-.029	40 - 60 knots	TSS, Sequential @2
4.	calct003.030-.053	40 - 60 knots	TSS, Sequential @2 Trip on 7
5.	calct003.054-.078	40 - 60 knots	TSS, Sequential @2 Stalls
6.	No Data	70 - 80 knots	Battery Failure
7.	No Data	60 - 80 knots	Battery Failure
8.	calct008.000-.034	40 - 80 knots	SDS at leading edge Straight and level & left and right turns.
9.	calct009.000-.031	40 - 80 knots	TSS, Alternate @4
10	calct010.000-.040	40 - 80 knots	SDS at leading edge Straight and level & left and right turns. Stalls.
11	No data	40 - 80 knots	Battery Failure

Table II. The Flight Test Chronology

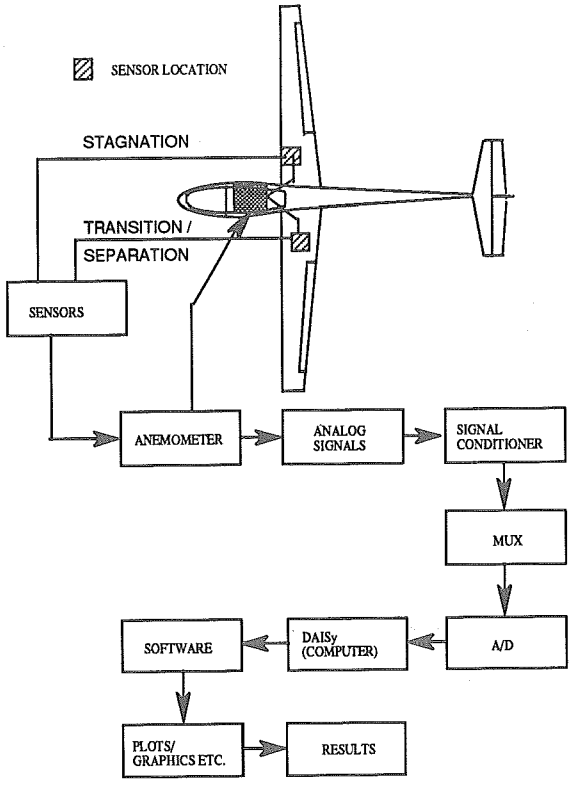

Figure 1. The flight test setup of the sensors, the sailplane and the DAISy.

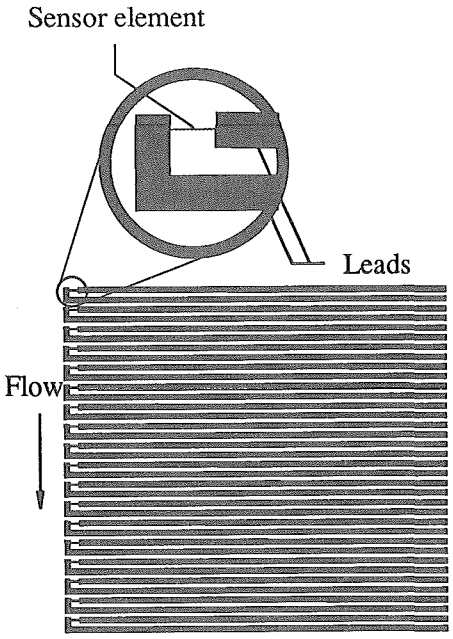

Figure 2. The multielement sensor configuration.

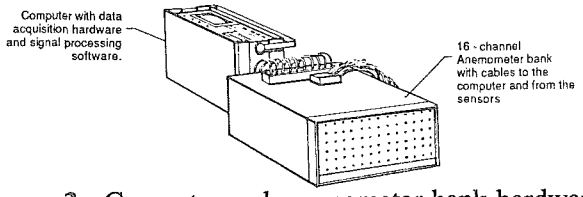

Figure 3. Computer and anemometer bank hardware setup used in the flight test.

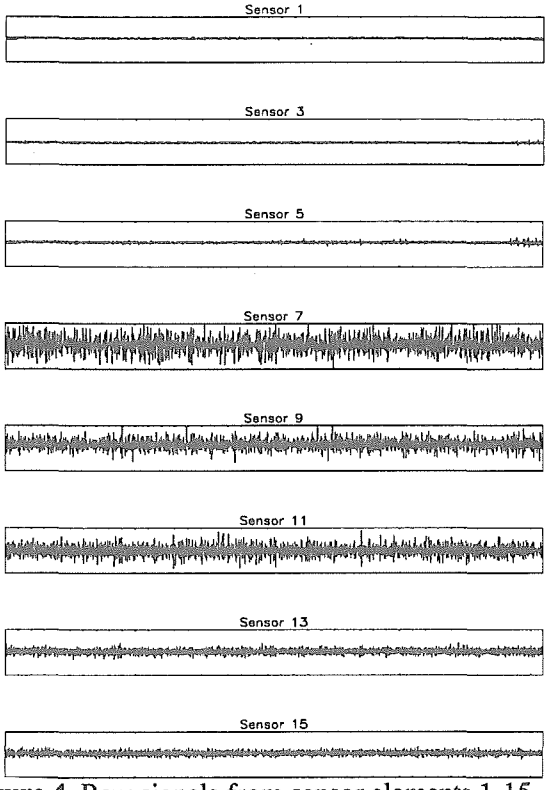

Figure 4. Raw signals from sensor elements 1-15 Flight 1, Run 11, Set 3) showing laminar to turbulent transition.

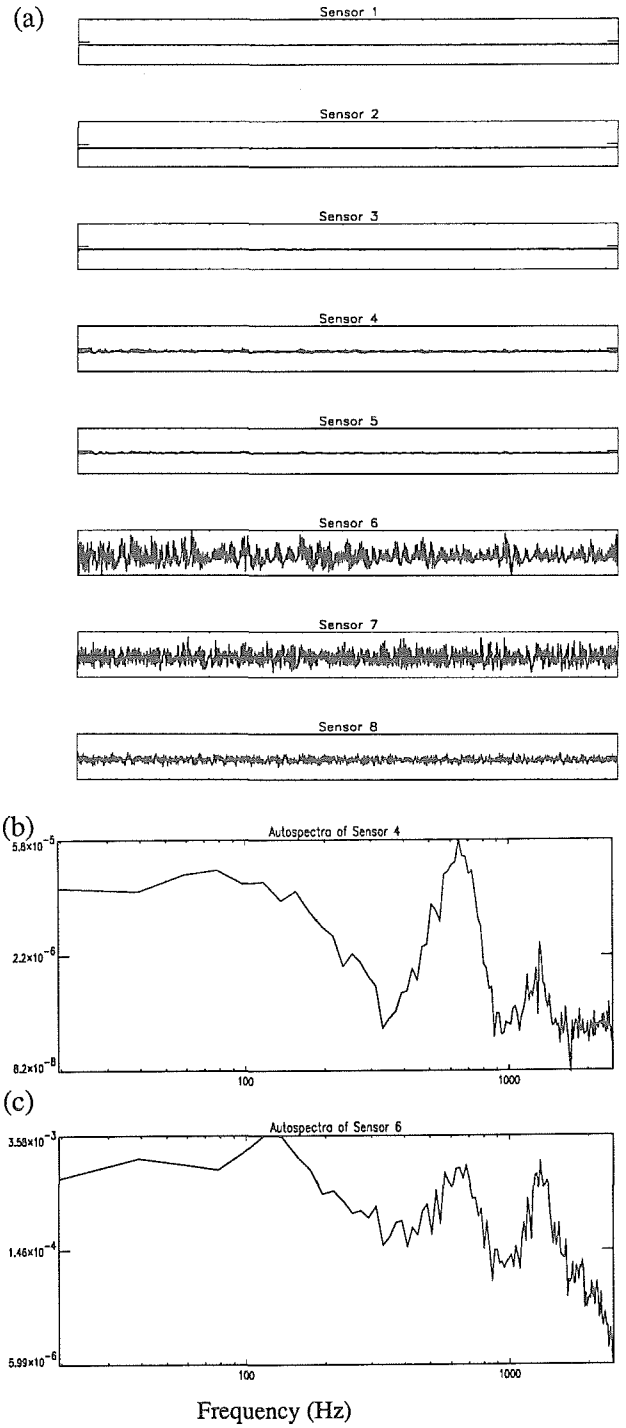

Figure 5. Raw signals from sensor elements 1-8 and autospectra plots for signals from (b) sensor 4 & (c) sensor 6 (Flight 1, Run 12, Set 1). Amplified T-S frequency : 650 Hz. Sailplane speed : 40 knots.

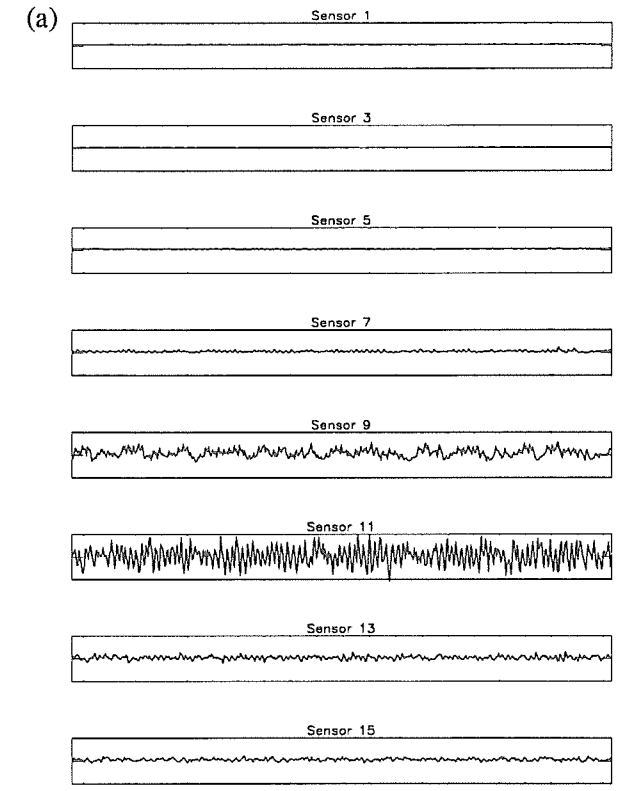

Figure 6. (a) Raw signals from sensor elements 1-15 and (b) autospectra plots for signals from sensors 7, 9, 11 & 13. (Flight 1, Run 19, Set 3). Amplified T-S frequency : 1000 Hz. Sailplane speed : 50 knots.

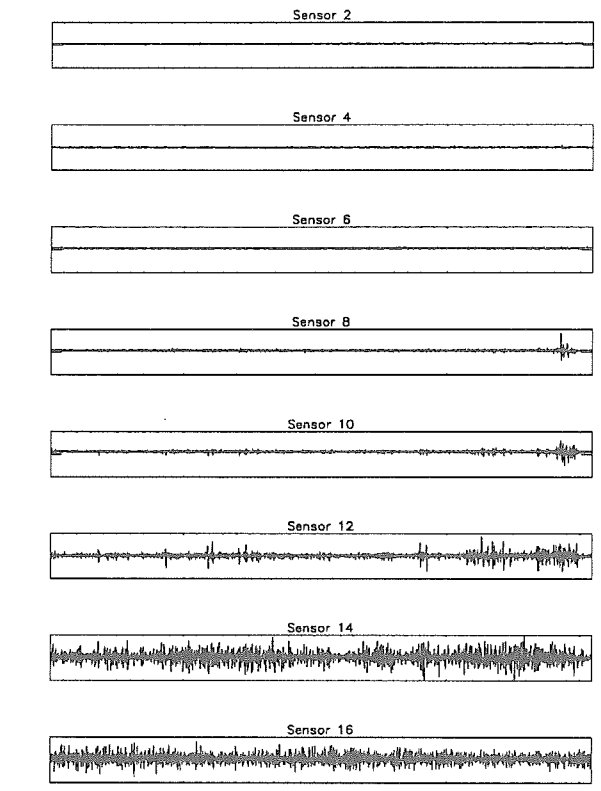

Figure 7. Signal traces from sensors 2-16 (Flight 3, Run 12, Set 7), showing laminar to turbulent transition, beginning at sensor 6. Peak transition location at sensor 14. (See Figs. 8 & 9 also).

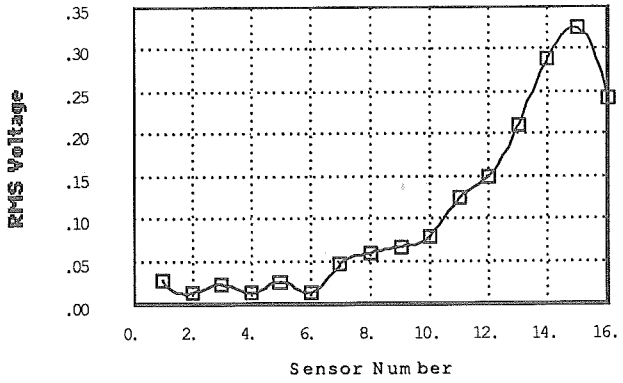

Figure 8. The RMS voltage distribution (Flight 3, Run 12).

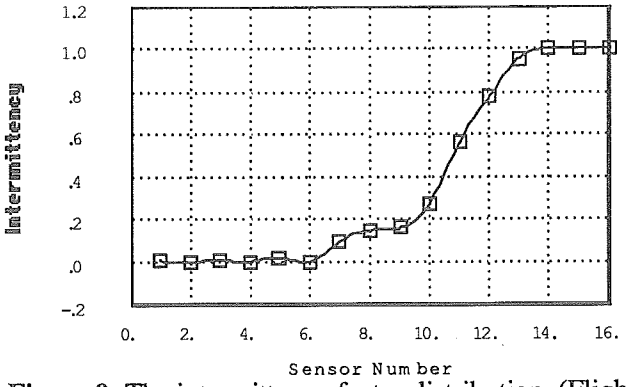

Figure 9. The intermittency factor distribution (Flight 3, Run 12).

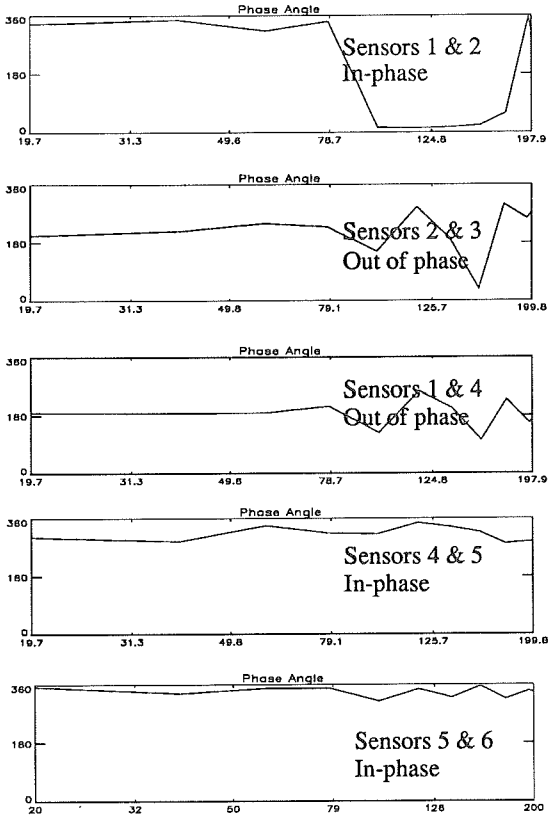

Figure 10. Phase angle plots from spectral analysis (Flight 1, Run 12, Set 1), showing separation location between sensors 2 & 3. (See Fig. 5(a) for raw signals).

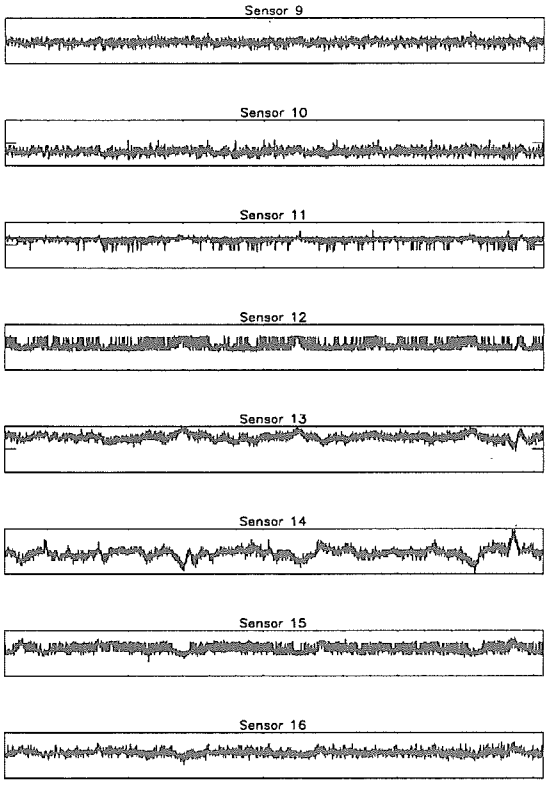

11 (a)

(b)

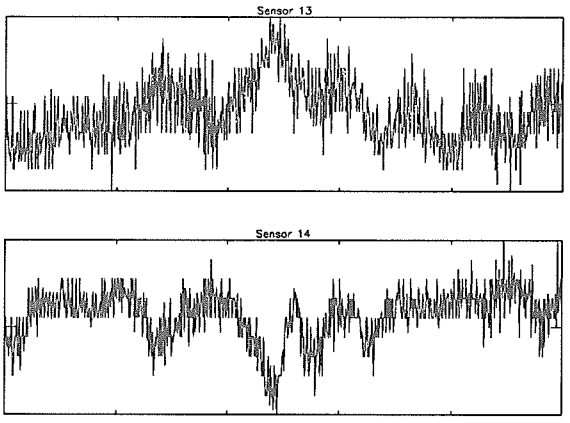

Figure 11. (a) Raw signals from sensor elements 9-16 (Flight 8, Run 10, Set 6), (b) A look at a small time segment from Fig. 11(a) to indicate phase reversal.

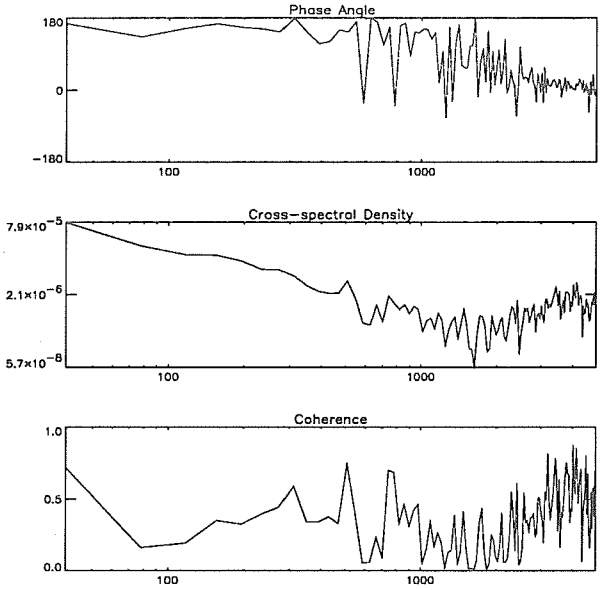

Figure 12. Cross-spectral analysis of the signals from sensors 13 and 14 (see Fig. 11). Note 180° phase difference between the signals.

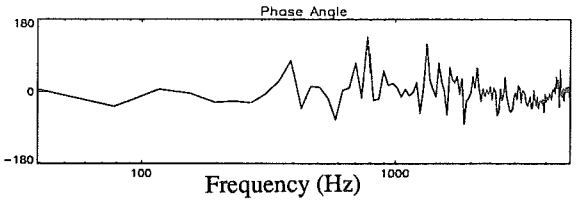

Figure 13. Phase relations between the signals from sensors 12 and 13 (see Fig. 11) showing in-phase signals.

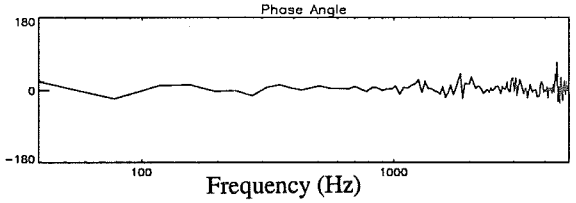

Figure 14. Phase relations between the signals from sensors 14 and 15 (see Fig. 11) showing in-phase signals.

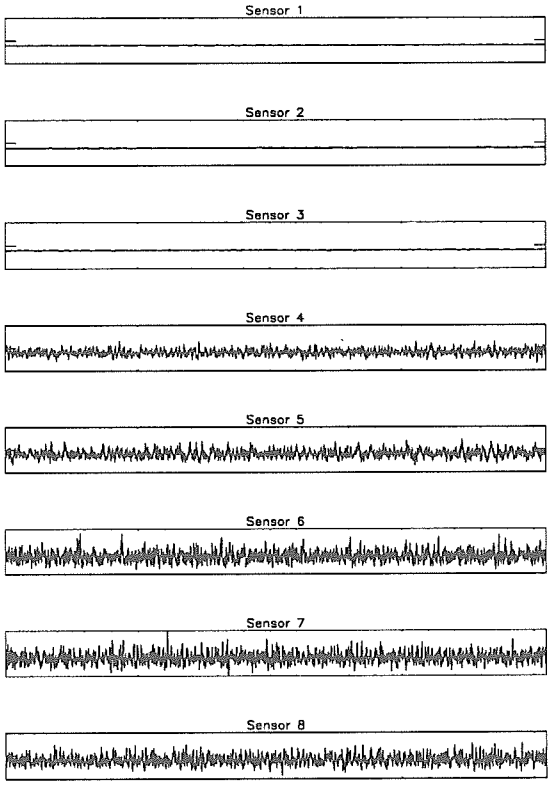

Figure 15. The effect of roughness located near sensor element 3 on sensor signals (Flight 9, Run 12, Set 5).

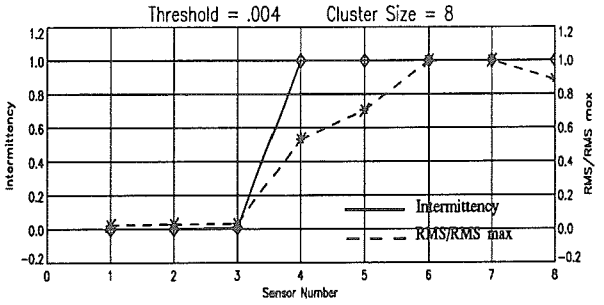

Figure 16. RMS and intermittency factor distribution for the data shown in Fig. 15.

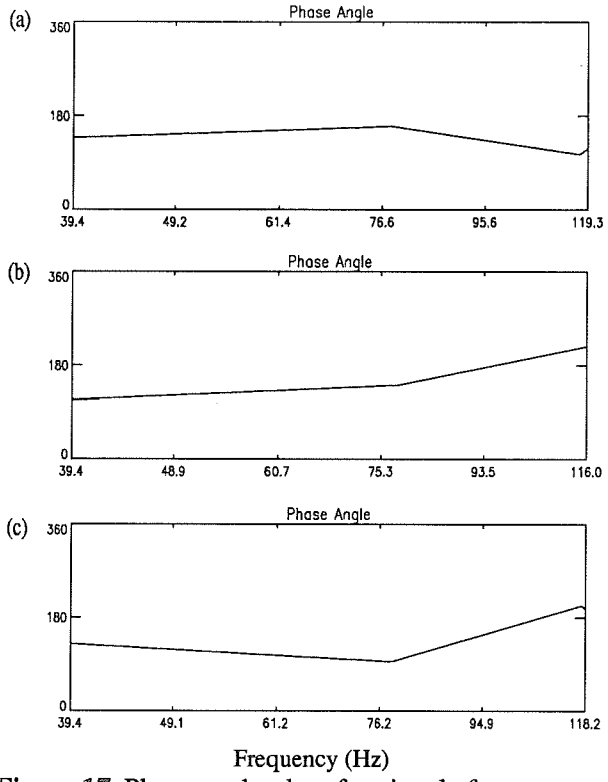

Figure 17. Phase angle plots for signals from sensor elements (a) 3 & 4, (b) 5 & 11 and (c) 7 & 11, (Flight 9, Run12).